Ionization of the one-dimensional Coulomb atom in an intense laser field

U. Schwengelbeck and F. H. M. Faisal

Fakultät für Physik, Universität Bielefeld, D-33615 Bielefeld, Germany

Interaction of the one-dimensional (1D) Coulomb atom with an intense radiation field is analyzed using the "hard" Coulomb potential $V_c(x) = -1/|x|$ and the "soft" Coulomb potential $V(x) = -1/\sqrt{x^2+1}$. Evolution of the probability wave packet and the photoelectron spectra is simulated numerically. In strong fields it is found (a) that the electron wave packet can break up into individual subpackets, (b) that there is a one-to-one correlation between the subpackets in space and the above-threshold-ionization peaks in energy, and (c) that a spatial confinement of the probability density can occur at a very high intensity. Finally, an example is given which indicates that the 1D "hard" Coulomb atom is less stable than the 1D "soft" Coulomb atom.

PACS number(s): 32.80.Rm

I. INTRODUCTION

Based on nonsingular atomic potentials of the form

$$V(x) = -1/\sqrt{x^2+1} \, , \qquad (1)$$

many papers (see, e.g., [1–3]) have been published investigating the dynamics of a model quantum system in one dimension interacting with a laser pulse [throughout this paper atomic units (a.u.) are used: $\hbar = e = m = 1$]. Such a model was suggested first some years ago by Eberly and collaborators [4] and is usually called the "soft" Coulomb potential. The potential (1) avoids numerical difficulties that usually occur at the origin $x = 0$ when dealing numerically with the one-dimensional singular Coulomb field

$$V_C(x) = -1/|x| \, . \qquad (2)$$

Recently, classical calculations of Grochmalicki, Lewenstein, and Rząźewski [5], Gajda *et al.* [6], and Ménis *et al.* [7] have shown that the form of the atomic potential strongly affects ionization: the more Coulomb-like the chosen binding potential, the higher the ionization probability. This leads to the question, what will be the effect on ionization, according to quantum dynamics, if the atom is described by the "hard" Coulomb potential (2)?

II. REGULARIZED COULOMB MODEL

The one-dimensional (1D) Coulomb model is defined by its Hamiltonian

$$\hat{H}_a(x) = \lim_{\alpha \to 0} -\frac{1}{2}\frac{\partial^2}{\partial x^2} - \frac{1}{|x|+\alpha} \qquad (3)$$

$$= -\frac{1}{2}\frac{\partial^2}{\partial x^2} - \frac{1}{|x|} \, . \qquad (4)$$

Loudon [8] has studied the eigenvalues and corresponding eigenfunctions of (4): it is shown that there exists a doubly degenerate set of normalized bound-state eigenfunctions with even ($\sigma = 0$) and odd ($\sigma = 1$) parity

$$\phi_n^\sigma(\alpha = 0, x) = \sqrt{2/n^3}\,|x|(\mathrm{sgn}(x))^\sigma$$

$$\times \exp\left\{-\frac{|x|}{n}\right\} {}_1F_1\left[1-n, 2, \frac{2|x|}{n}\right] \, , \qquad (5)$$

where $n = 1, 2, \ldots, \infty$ and the energy eigenvalues are

$$\epsilon_n(\alpha = 0) = -\frac{1}{2n^2} \, . \qquad (6)$$

In case of the continuous spectrum with positive-energy eigenvalues the wave function can be obtained by analytic continuation

$$n = -i/k \quad \text{with} \quad \epsilon(\alpha = 0, k) = k^2/2 \, . \qquad (7)$$

The eigenvalue with the lowest energy is not degenerate and depends logarithmically on α:

$$\epsilon_0(\alpha) \simeq -2\left[\ln\left[\frac{1}{\alpha}\right]\right]^2 \quad \text{for } \alpha \ll 1 \qquad (8)$$

and

$$\epsilon_0(\alpha \to 0) \to -\infty \, , \qquad (9)$$

implying an infinite binding energy which is clearly unphysical. The corresponding normalized eigenfunction (even parity) for $\alpha \ll 1$ is

$$\phi_0(\alpha, x) \simeq \frac{\exp(-|x|/\alpha)}{\sqrt{\alpha}} \, . \qquad (10)$$

Thus, except the lowest (unphysical) state that satisfies $|\phi_0(0,x)|^2 = \delta(x)$, all eigenfunctions of (4) vanish at the origin.

We now introduce a formal definition of a one-dimensional "hard" Coulomb model with the Hamiltonian

$$\hat{H}_a^r(x) = \lim_{\alpha \to 0} -\frac{1}{2}\frac{\partial^2}{\partial x^2} - \frac{1}{|x|+\alpha} - |\phi_0\rangle\epsilon_0\langle\phi_0| \, . \qquad (11)$$

The projection operator $-|\phi_0\rangle\epsilon_0\langle\phi_0|$ in (11) eliminates the unphysical state ϕ_0 and ensures that all energy eigen-

values are similar to those of 3D hydrogen atoms where $\epsilon_0(\alpha=0)$ does not occur. Note that, in contrast to the "soft" Coulomb model, the "hard" Coulomb model (11) allows degeneracy of energy eigenvalues as does three-dimensional hydrogen. Note also that the present model, unlike the Coulomb model defined on the half axis [9,10], retains parity as a good quantum number.

The time-dependent interaction

$$\hat{H}_i(x,t)=-xE(t) \tag{12}$$

describes the influence of the laser field $E(t)=E_0f(t)\sin(\omega t)$ in dipole approximation. E_0 denotes the peak amplitude, $f(t)$ the envelope, and ω the frequency of the electric field.

To study the dynamics of the "hard" Coulomb model in the laser field, we are interested in the solution of the time-dependent Schrödinger equation

$$i\frac{\partial}{\partial t}\psi(x,t)=[\hat{H}_a^r(x,t)-xE(t)]\psi(x,t) \ , \tag{13}$$

where an initial wave function $\psi(x,0)=\phi_n^\sigma(x)$ with $n=1,2,\ldots,\infty$ is given. The solution can be computed numerically most conveniently from

$$i\frac{\partial}{\partial t}\psi(x,t)= \left[-\frac{1}{2}\frac{\partial^2}{\partial x^2}-\frac{1}{|x|}-xE(t)\right]\psi(x,t) \ , \quad \forall x\neq0 \ ,$$

$$\psi(0,t)=\psi(0,0) \ \ \forall t \ . \tag{14}$$

A mathematical demonstration that Eq. (14) is equivalent to Eq. (13) is given in the Appendix. The reader should note that an initial state that is zero at the origin at the time $t=0$ evolves into a state that remains zero at $x=0$ at all times [see Appendix, Eq. (A6)]. Furthermore this time-dependent solution remains orthogonal to ϕ_0 (the unphysical ground state of the nonregularized Hamiltonian) at all times [Eqs. (A7) and (A14)]. For the numerical integration of (14), we have used a finite-difference representation where the time derivative is given by a two-point scheme of second-order accuracy, and the second-order derivative in space is given by a five-point difference scheme of fourth-order accuracy (cf. [11]).

III. RESULTS AND DISCUSSION

In the rest of this work we use both the "hard" Coulomb and the "soft" Coulomb model to investigate a number of phenomena in laser-atom interactions in intense fields. We report on (a) the splitting of the electron wave into subpackets, (b) a one-to-one correlation of the subpackets in space with the individual above-threshold-ionization (ATI) peaks in energy, and (c) a form of "localization" or "confinement" in which the extension of the electron wave packet for a high laser intensity is more "confined" in space than that at a lower intensity, followed by a "dispersion" of the wave packet during the tail of the pulse. Ionization probability for different laser intensities is also investigated, and an example of the difference in the survival probability calculated with the "hard" Coulomb model and the "soft" Coulomb model is given, which indicates lesser "stability" of the former sys-
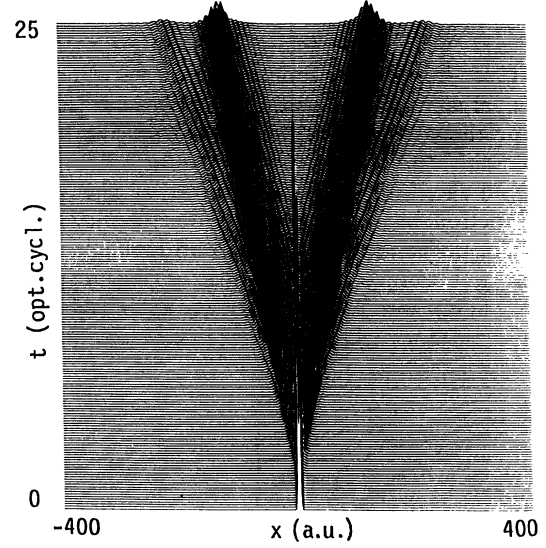

FIG. 1. Probability density $|\psi(x,t)|^2$ of the "hard" Coulomb atom in the laser field; $\omega=1$ (a.u.) and $E_0=0.5$ (a.u.) (perpendicular perspective).

tem compared to the latter.

In the present investigation the frequency of the laser field, $E(t)=E_0f(t)\sin(\omega,t)$, is chosen to be $\omega=1$ (a.u.) (45.563 nm), which lies in the ultraviolet region. In this case the energy of one photon is sufficient for ionization (a nominal one-photon process). Furthermore we choose an electric field envelope

$$f(t)= \begin{cases} \sin^2\{\pi t/(2\tau)\} \ , & 0<t<\tau \\ 1 \ , & \tau\leq t\leq T-\tau \\ \cos^2\{\pi(t+\tau-T)/(2\tau)\} \ , & T-\tau<t<T \end{cases} \tag{15}$$

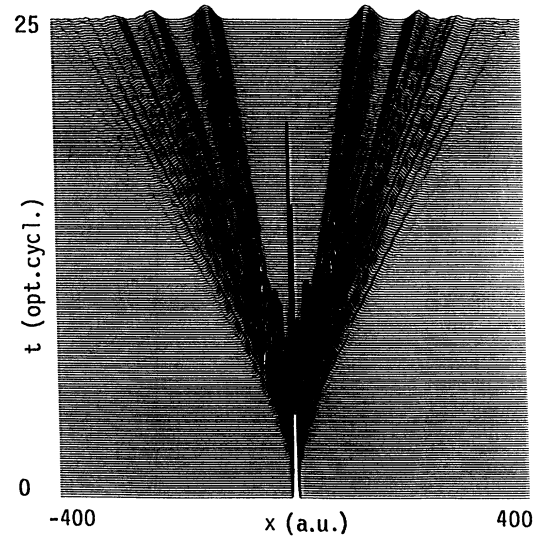where T denotes the pulse duration (25 optical cycles)

FIG. 2. Same as Fig. 1, but $E_0=1$ (a.u.).

and τ the time for turning on and the turning off (five optical cycles each) of the field. The solution is propagated with a given initial wave function $\psi(x,t=0)$. The numerical convergence of the solution has been tested first by changing the step sizes in time and space and by moving the boundary to higher $|x|$ values, until reflection effects were eliminated. Finally, the norm of the converged wave function has been checked during the simulation and has been found to be accurate to within a maximum error of less than 0.2%. In case of the field strength $E_0 = 0.5$ (a.u.) and $E_0 = 1$ (a.u.) we have taken 400 000 discrete time steps and a spatial step size $\delta x = 0.1$ (a.u.) in

the difference scheme, whereas for $E_0 = 10$ (a.u.) we have found 2 400 000 discrete time steps and $\delta x = 0.1$ (a.u.) to be sufficient for convergence. For simulations shown in Figs. 1, 2, and 3(a), a maximum value $|x_{\max}| = 400$ (a.u.) has been found to be sufficient to eliminate any boundary reflections.

To check whether alternative schemes of regularization of the Coulomb model give different results or not, we have compared the results, based on the analytic regularization (14) and the results obtained from two other numerical limiting procedures where (i) the potential parameter α has been decreased systematically, until the re-
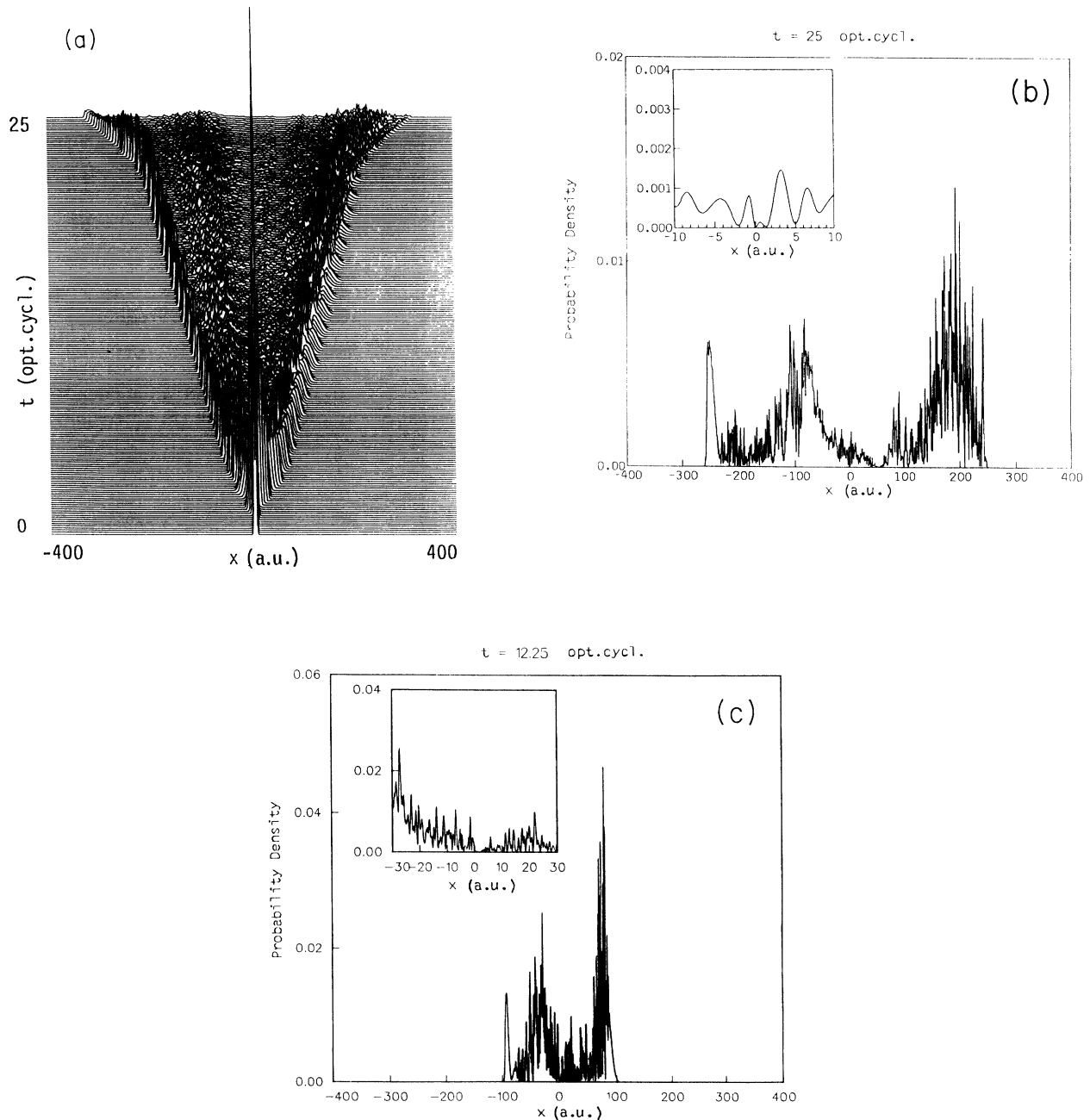

FIG. 3. (a) Same as Fig. 1, but $E_0 = 10$ (a.u.). (b) Probability density at time $t = 25$ (optical cycles); $\omega = 1$ (a.u.), $E_0 = 10$ (a.u.). (c) Same as in (b), but $t = 12.25$ (optical cycles).

sults have become independent of α; and (ii) the Coulomb potential V_C has been cut off at the origin with increasing depths, until the results have become independent of the cutoff depth. The results of these two comparative computations have been found to be indistinguishable from those obtained from (14) for $\alpha \leq 2 \times 10^{-3}$ and/or for cutoff depths of the potential ≤ -500.

Physically this result can be understood in terms of the negligible probability for a laser-induced transition from an initial bound state (e.g., ϕ_1) to the unphysical state ϕ_0 if the parameter α is close to zero [in case of $\alpha = 2 \times 10^{-3}$ the energy difference for such a transition is according to (8) about 77 (a.u.) or 2079 eV]. When α is small enough, it is expected therefore that the contribution of ϕ_0 would be negligible and the results would be numerically equivalent to those of the "hard" Coulomb model where $\alpha = 0$ and ϕ_0 is projected away from the spectrum. This expectation is fully substantiated by the converged results according to the three different procedures discussed above. We may note parenthetically that spontaneous (i.e., not induced) transitions are not considered in our simulations.

The wave function in the case of the "hard" Coulomb atom is propagated with the initial state

$$\phi_1^{\sigma=1}(x) = \sqrt{2}x \exp(-|x|) , \tag{16}$$

corresponding to an energy $\epsilon_1 = -0.5$ which is equal to the ground-state energy eigenvalue of the ordinary hydrogen atom. It should be remarked that the initial state chosen in this simulation has odd parity ($\sigma = 1$), and results of calculations beginning with an even state are qualitatively analogous. The probability densities $|\psi(x,t)|^2$ of the atomic electron in the three different laser fields with peak amplitudes $E_0 = 0.5$ (a.u.), $E_0 = 1$ (a.u.), and $E_0 = 10$ (a.u.) (intensities in the range 8.75×10^{15} W/cm^2–3.5×10^{18} W/cm^2) are shown in Figs. 1, 2, and 3(a), respectively. The corresponding electron energy spectra are presented in Figs. 4, 5, and 6. The photoelectron spectra for $E_0 = 0.5$ (a.u.) (Fig. 4) and $E_0 = 1$ (a.u.) (Fig. 5) show kinetic-energy distributions that are typical for the so-called above-threshold ionization (ATI) [15] for high incident laser intensities: in both spectra there are sequences of peaks, separated by the photon energy $\omega = 1$ (a.u.), i.e., at high intensities the atom absorbs more photons than are actually necessary for ionization. For the field amplitude $E_0 = 10$ (a.u.) we find a photoelectron spectrum with a broad energy distribution with complex fine structures (Fig. 6).

Pont et al. [12] and Kulander, Schafer, and Krause [13] have found in 3D calculations a "dichotomous" peak splitting of the wave function with separations of the order of the "quiver radius" $\alpha_0 = E_0 / \omega^2$ (a.u.). This phenomenon has also been observed by Su, Eberly, and Javanainen [2] and Reed, Knight, and Burnett [3] in calculations in the space translated (Kramers-Henneberger) frame [14] with the "soft" Coulomb model, where a two or more peaked spatial distribution has been found. For the present calculation with the "hard" Coulomb model, we have found a multiple splitting of the spatial electron distributions at high laser intensities as shown in Figs. 1
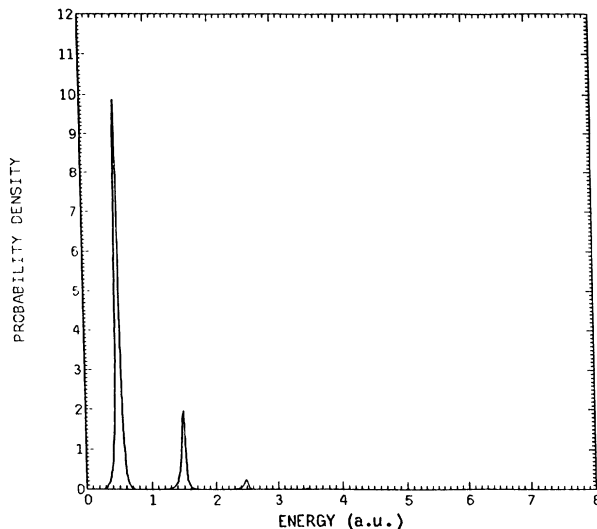

FIG. 4. ATI spectrum of the "hard" Coulomb atom in the laser field; $\omega = 1$ (a.u.) and $E_0 = 0.5$ (a.u.).
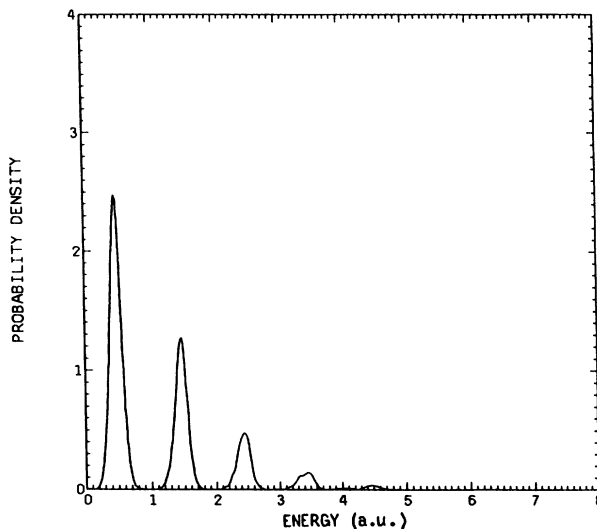

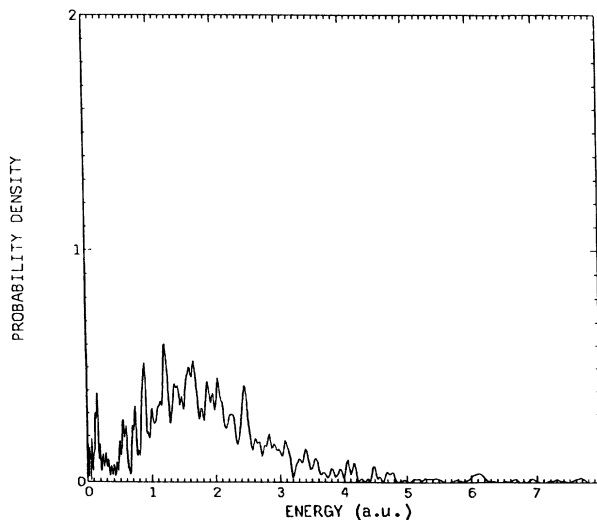FIG. 5. Same as Fig. 4, but $E_0 = 1$ (a.u.).

FIG. 6. Same as Fig. 4, but $E_0 = 10$ (a.u.).

and 2. It is seen that electron subpackets appear that are separated asymptotically by much larger distances than α_0. What is the physical significance of this phenomenon? We interpret this as a spatial grouping of the ATI electrons by establishing a one-to-one correlation between the individual spatial subpackets *inside the field* and the individual peaks in the ATI energy spectra. This is evidenced in Fig. 7, which brings together the spatial atomic probability distribution $|\psi(x,t)|^2$ shown in Fig. 2 and the corresponding energy distribution shown in Fig. 5. It is seen that each particular subpacket asymptotically moves with a velocity $v = \Delta x / \Delta t$, which can be read off from the slope of the line defining the motion of the crest of the particular subpacket. The associated kinetic energies $v^2/2$ turn out to be equal to the energies of the corresponding ATI peaks (indicated in Fig. 7 by an arrow). This correlation is also shown quantitatively in Table I. Thus we are able to identify the motion of the ATI electrons in space with individual subpackets of the probability density $|\psi(x,t)|^2$. Note that the subpackets traveling on the left-hand side of the origin are associated with negative values of v's but correspond to the same energies of the ATI peaks as shown above. An exactly
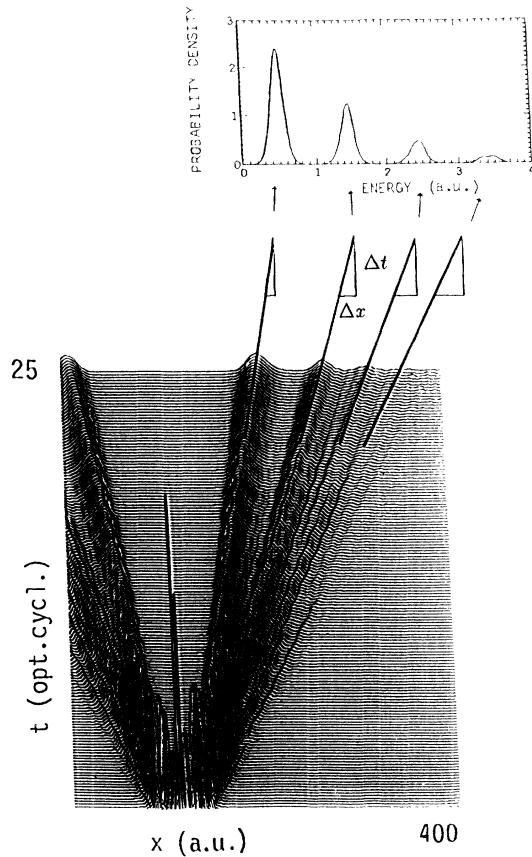
TABLE I. Velocities $v = \Delta x / \Delta t$ and the associated kinetic energies $v^2/2$ of the electron probability subpackets in the laser field where $E_0 = 1$ (a.u.) and $\omega = 1$ (a.u.). The associated kinetic energies can be identified with the energies ϵ_S of the individual peaks in the ATI spectrum.

S	Δt	Δx	$v = \Delta x / \Delta t$	$v^2/2$	ϵ_S
0	16.0	15.6	0.98	0.48	0.48
1	16.0	27.5	1.72	1.48	1.48
2	16.0	35.6	2.23	2.49	2.48
3	16.0	42.2	2.64	3.49	3.48

analogous correlation exists between the spatial subpackets in Fig. 1 and the ATI peaks in Fig. 4, corresponding to $E_0 = 0.5$ (a.u.), $\omega = 1$ (a.u.). For very high intensities, the ATI peaks tend to smear out into a broad distribution, but even then a trace of the same correlation may be detected as seen between Figs. 3(a) and 6 for $E_0 = 10$ (a.u.), $\omega = 1$ (a.u.). In this case of a very intense laser field with $E_0 = 10$ (a.u.), we also observe a form of "localization" or "confinementlike" behavior in Fig. 3(a): the electron probability in space is now confined within only about *half* the distance from the origin than for the lower intensities (Figs. 1 and 2), for the same duration of the pulse. An even more pronounced "confinement" effect is seen in case of the "soft" Coulomb atom (see Fig. 11 below). Another interesting effect seen in this case is that the wave packet tends to "disperse" during the last five cycles when the field is switched off. In the present parameter domain, this effect is found to be not very significant in case of the "soft" Coulomb model (cf. Fig. 11 below). We note that this phenomenon is numerically stable, but requires further investigation regarding its physical significance or otherwise. In Fig. 3(b) we show the probability density distribution at the end of the pulse in the (laboratory frame) along with a magnified view near the origin (see inset). It shows no presence of the so-called "dichotomy" and the peak values of the density are an order of magnitude smaller near $|x| \simeq \alpha_0$ or $2\alpha_0$ than at much larger distances. Figure 3(c) shows the probability density near the midpoint of the pulse [when the field amplitude $E(t) = 10$ (a.u.) and the corresponding quiver energy is 680 eV] along with a magnified view, within 30 (a.u.) from the nucleus, given in the inset. In this case too there is no clear sign of a "dichotomous" behavior near $|x| \simeq \alpha_0$ or $2\alpha_0$.

The total ionization probability of the "hard" Coulomb atom interacting with the laser field is investigated using the definition

$$P_{\text{ion}}(t) = 1 - \sum_{n=1}^{\infty} \sum_{\sigma=0}^{1} P_n^{\sigma}(t) , \qquad (17)$$

where

$$P_n^{\sigma}(t) = |\langle \psi(t)|\phi_n^{\sigma}\rangle|^2 . \qquad (18)$$

In our commutations the sum in (17) is taken over the first 100 bound states with $n = 1, \ldots, 50$ (each with even and odd parity). Contributions from $P_n^{\sigma}(t)$ for $n > 50$ are found to be negligible.
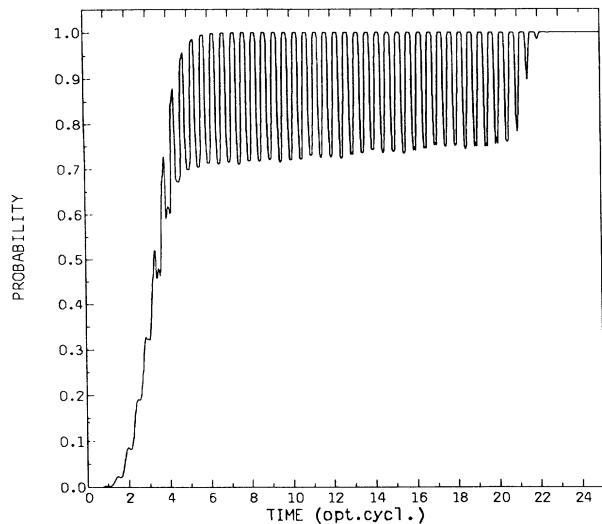

FIG. 7. Correlation between spatial subpackets, formed by wave-packet splitting, and the ATI peaks [$\omega = 1$ (a.u.) and $E_0 = 1$ (a.u.)]. The crest of each subpacket of the electron probability density moves with a velocity $v = \Delta x / \Delta t$; the associated kinetic energy $v^2/2$ can be identified with the energy of an individual peak in the ATI spectrum (indicated by an arrow).

FIG. 8. Ionization probability of the "hard" Coulomb atom in the laser field; $\omega = 1$ (a.u.) and $E_0 = 1$ (a.u.).
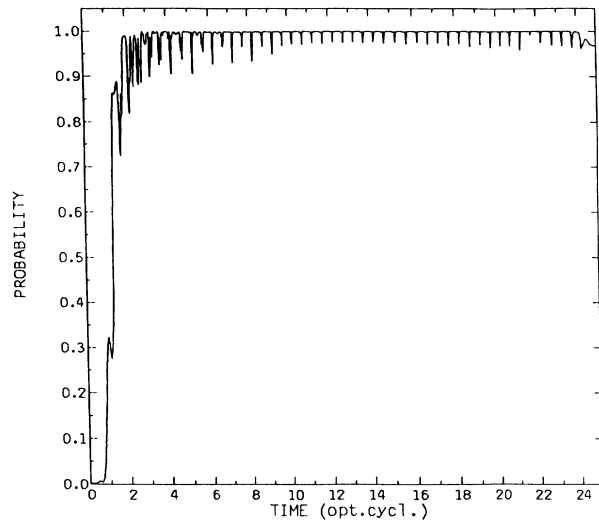
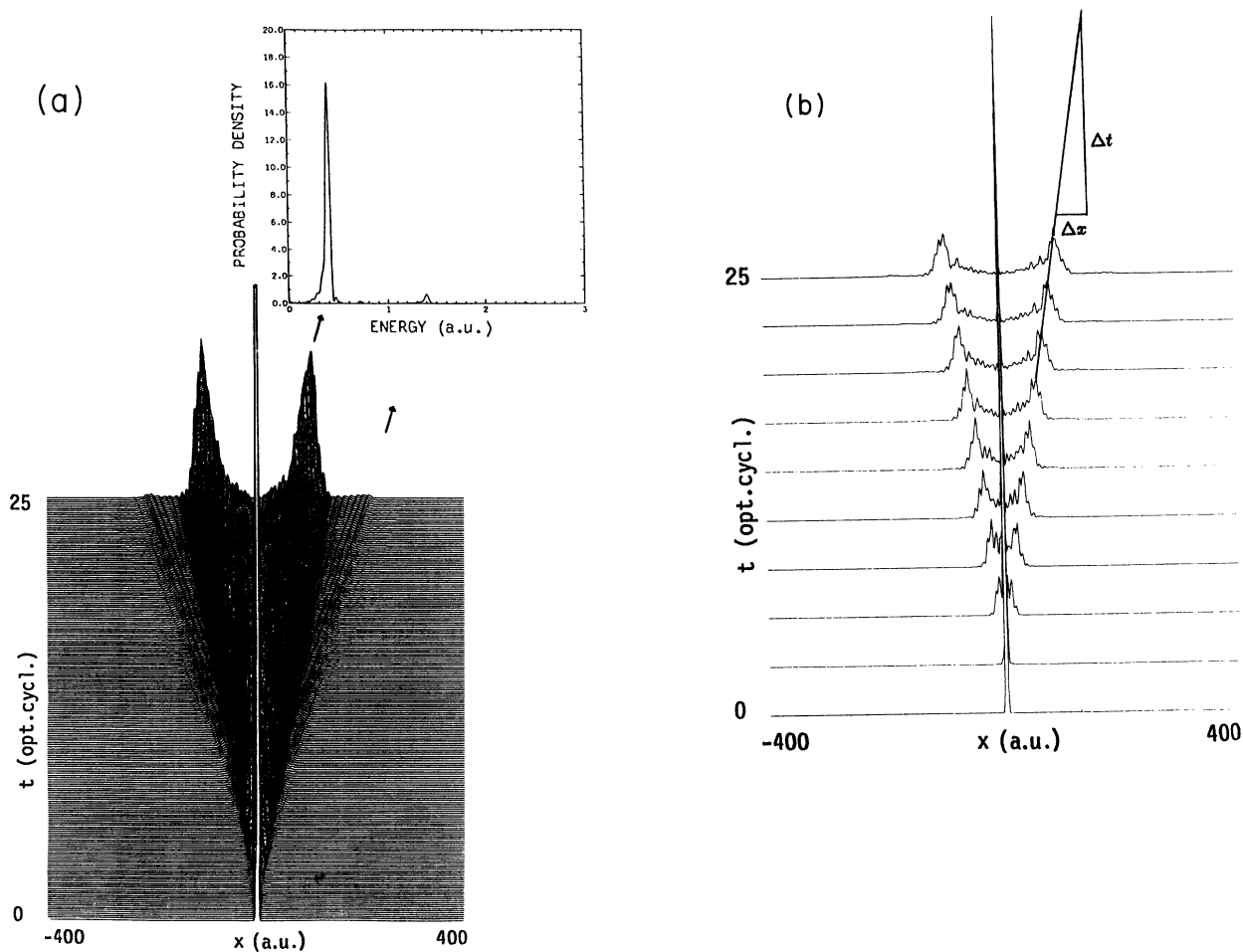FIG. 9. Same as Fig. 8, but $E_0 = 10$ (a.u.).

FIG. 10. (a) Probability density $\psi(x,t)|^2$ and the corresponding ATI spectrum of the "soft" Coulomb model; $\omega = 1$ (a.u.) and $E_0 = 1$ (a.u.). (b) Probability density as in (a), but with a reduced vertical scale and fewer time steps, which reveals the linear motion of the high-density group of the wavepackets more clearly.

For $E_0 = 1$ (a.u.) the laser interaction leads to an oscillation of the ionization probability and ends with a complete ionization of the atom as shown in Fig. 8; at the end of the process there are no electrons left in bound states with negative energy. In Fig. 9 the ionization probability is shown for $E_0 = 10$ (a.u.). After only a few optical cycles the laser-atom interaction leads to a continuum population equal to unity, but as in the previous case with increasing time, the atom periodically returns to bound states and finally ends with a nearly complete ionization ($\simeq 97\%$). Thus in relation to the process where $E_0 = 1$ (a.u.), the atom appears to be somewhat more stable at the higher field strength $E_0 = 10$ (a.u.). This phenomenon is correlated to the confinement of the probability density in space, we have mentioned above.

To make sure that the phenomena of (a) the breaking up of the wave function into subpackets, (b) the one-to-one correlation between spatial subpackets and ATI peaks, and (c) the tendency of "confinement" of the probability density in space at very high laser intensity are not peculiarities of the "hard" Coulomb atom, we have carried out a sequence of simulations with the "soft" Coulomb model.

In Fig. 10(a) the electron density distribution for the "soft" Coulomb atom in the laser field with $E_0 = 10$ (a.u.) is compared with the corresponding ATI spectrum. As in the simulation with the "hard" Coulomb atom, the electron density breaks up into subpackets, which again can be correlated one-to-one with the main peaks in the energy spectrum. In Fig. 10(a), the motion of the low-density group of the subpackets can be observed clearly. In contrast to the low-density group, the high-density group is rather obscured due to the choice of the scale. The motion of the high-density group is resolved more clearly by reducing the vertical scale and thinning out the time steps as shown in Fig. 10(b). The estimated velocities v and the associated kinetic energies $v^2/2$ are compared with the energies ϵ_S of the ATI peaks in Table I, which shows the one-to-one correlation as noted above for the "hard" Coulomb atom We conclude that the correlation between the subpackets in space and the ATI peaks in the energy spectrum is essentially independent of the chosen atomic model.

In Fig. 11 we show the spatial electron density obtained by a simulation with the "soft" Coulomb atom at the very high field strength $E_0 = 10$. As in the case of the "hard" Coulomb atom (cf. Fig. 3), the wave packet at $E_0 = 10$ is seen to be confined closer to the origin ($|x_{max}| \simeq 100$) than in the case of the lower field strength $E_0 = 1$ ($|x_{max}| \simeq 200$). On the other hand, as mentioned above, the strong "dispersive" effect (seen near the end of the pulse in case of the "hard" Coulomb model) is rather negligible in the case of the "soft" Coulomb model.

Finally we have considered the survival probability (i.e., the probability to find the atom in its initial state)

$$P_1(t) = |\langle \psi(t) | \phi_1^\sigma \rangle|^2 , \tag{19}$$

using the 1D "hard" Coulomb atom, which is shown in Fig. 12. It is seen that $P_1(t)$ oscillates with increasing time and tends to zero after only a few optical cycles.
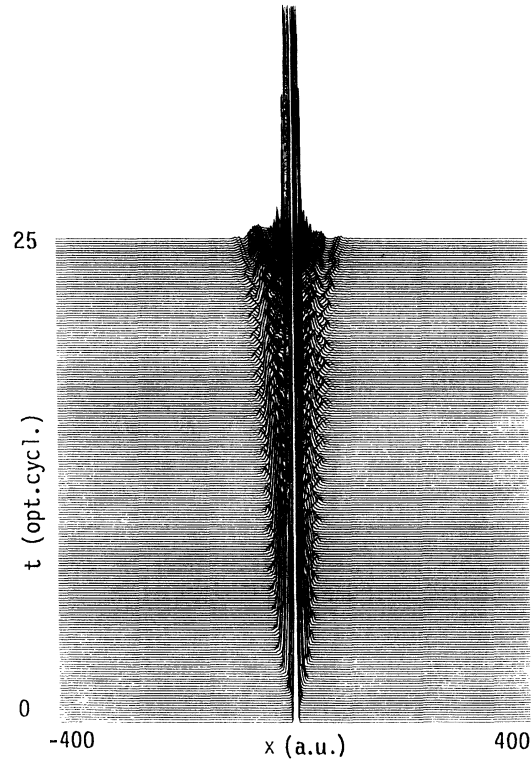

FIG. 11. Probability density $|\psi(x,t)|^2$ of the "soft" Coulomb atom in the laser field; $\omega = 1$ (a.u.) and $E_0 = 10$ (a.u.).

The oscillations of the survival probability and the ionization probability indicate repeated bound-free transitions, especially from the initial state to continuum states and vice versa, until the pulse is over. Whether the oscillations of the probability (computed in the laboratory frame) will have measurable consequences is an interesting question whose answer would depend on possible ex-
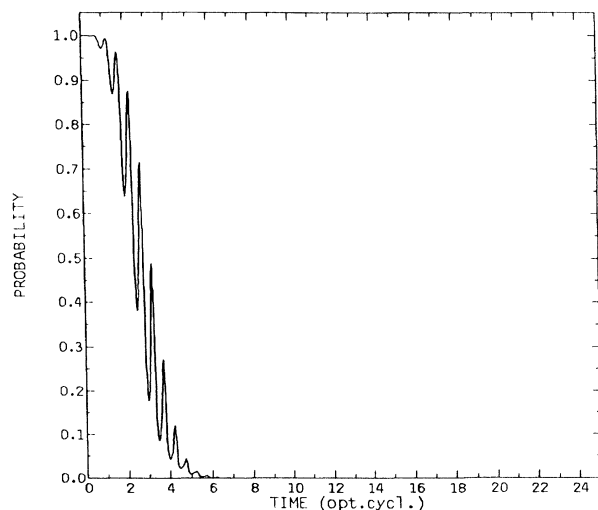

FIG. 12. Survival probability of the "hard" Coulomb atom in the laser field; $\omega = 1$ (a.u.) and $E_0 = 1$ (a.u.).
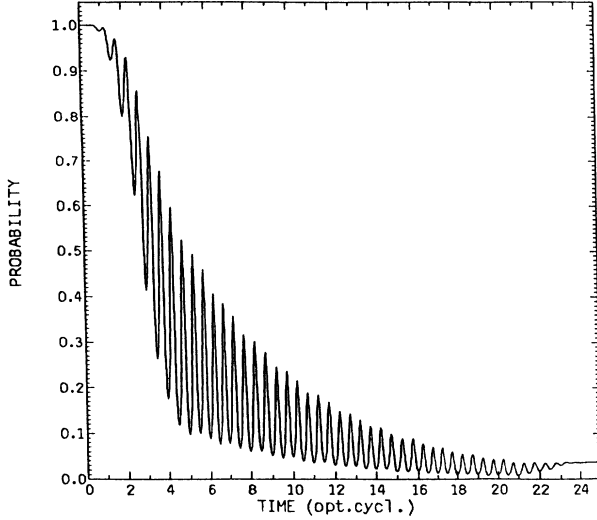
FIG. 13. Survival probability of the "soft" Coulomb atom in the laser field; $\omega = 1$ (a.u.) and $E_0 = 1$ (a.u.).

perimental arrangements to observe the time evolution of the system and may not be ruled out *a priori*.

We have also found indications that in contrast to the "hard" Coulomb atom, the "soft" Coulomb atom in the laser field is more stable. This is consistent with the recent findings of classical simulations [5–7]. To give an example, in Fig. 13 the survival probability of the "soft" Coulomb atom is shown, where the same pulse as used for the "hard" Coulomb atom (cf. Fig. 12) has been chosen. It is seen that the probability of finding the "soft" Coulomb atom at the end of the pulse in its initial state is nearly 4%, while the "hard" Coulomb atom has no probability of survival in the initial state.

To summarize, we have introduced a regularized 1D "hard" Coulomb atomic model that provides energy eigenvalues analogous to that of the 3D hydrogen atom. Numerical investigations of the interaction of the "hard" and the "soft" Coulomb atom with intense laser pulses reveal a highly nonperturbative phenomenon of multiple splitting of the atomic wave packet into individual subpackets in space, which are correlated one-to-one with the ATI peaks in the energy domain. A spatial confinement of the wave packet at a very strong field is observed. Finally, the quantum 1D "hard" Coulomb atom is found to be less stable than the quantum 1D "soft" Coulomb atom, which supports recent findings within classical simulations.

ACKNOWLEDGMENTS

APPENDIX

In this appendix, we show the equivalence of the Schrödinger equations (13) and (14). On expanding the time-dependent wave function in atomic eigenstates

$$\psi(x,t) = \sum_{n=0}^{\infty} \sum_{\sigma=0}^{1} c_n^{\sigma}(t)\phi_n^{\sigma}(x) \tag{A1}$$

(where in case of continuum states the sum is interpreted as an integral) and substituting expression (A1) in the right-hand side of the Schrödinger equation,

$$i\frac{\partial}{\partial t}\psi(x,t) = [\hat{H}_a^r(x,t) - xE(t)]\psi(x,t) , \tag{A2}$$

where

$$\hat{H}_a^r(x) = -\frac{1}{2}\frac{\partial^2}{\partial x^2} - \frac{1}{|x|} - |\phi_0\rangle\epsilon_0\langle\phi_0| , \tag{A3}$$

one obtains

$$i\frac{\partial}{\partial t}\psi(x,t) = \sum_{n=1}^{\infty} \sum_{\sigma=0}^{1} [\epsilon_n - xE(t)]c_n^{\sigma}(t)\phi_n^{\sigma}(x) . \tag{A4}$$

Note that the $n = 0$ term has canceled out exactly and does not appear in Eq. (A4), as a result of (A3). Multiplication of Eq. (A4) with $\delta(x)$ and integration over x leads to

$$i\frac{\partial}{\partial t}\psi(0,t) = \int_{-\infty}^{\infty} dx \sum_{n=1}^{\infty} \sum_{\sigma=0}^{1} \delta(x)(\epsilon_n - xE(t))c_n^{\sigma}(t)\phi_n^{\sigma}(x)$$

$$= \sum_{n=1}^{\infty} \sum_{\sigma=0}^{1} c_n^{\sigma}(t)\phi_n^{\sigma}(0) = 0 . \tag{A5}$$

The last line follows in view of the fact that all eigenfunctions $\phi_n^{\sigma}(x)$ for $n \neq 0$ vanish at the origin ($x = 0$) and the amplitudes $c_n^{\sigma}(t)$ are finite quantities. Equation (A5) implies that

$$\psi(0,t) = \psi(0,0) . \tag{A6}$$

We note that $\psi(0,0) = 0$ if one of the states $\phi_n^{\sigma}(x)$ with $n \neq 0$ is taken as the initial state. The interested reader may note that the wave function $\psi(x,t)$ [solution of Eq. (A2)] which evolves from any of the initial states, belonging to the regularized Hamiltonian (A3), remains orthogonal to the unphysical state ϕ_0 at all times, i.e.,

$$I = \lim_{\alpha \to 0} \int_{-\infty}^{\infty} \phi_0(\alpha,x)\psi(x,t)dx = 0 , \quad \forall t . \tag{A7}$$

This can be seen as follows. Substitute (A1) for $\psi(x,t)$, so that

$$I = c_0^{\sigma}(t) , \tag{A8}$$

since

$$\langle \phi_0^{\sigma}|\phi_n^{\sigma'}\rangle = \delta_{n,0}\delta_{\sigma,\sigma'} . \tag{A9}$$

From Eq. (A6) we have

$$\psi(0,t) = \lim_{x \to 0} \psi(x,t)$$

$$= \lim_{\alpha \to 0}\lim_{x \to 0}\left[c_0^{\sigma}(t)\phi_0^{\sigma}(\alpha,x) + \sum_{n=1}^{\infty} \sum_{\sigma=0}^{1} c_n^{\sigma}(t)\phi_n^{\sigma}(x) \right] . \tag{A10}$$

The sum on the right-hand side goes to zero at least linearly with x as $x \to 0$. Therefore

$$\psi(0,t) = \lim_{x \to 0} c_0^\sigma(t)\phi_0^\sigma(\alpha,x) \qquad (A11)$$

and from (A6)

$$c_0^\sigma(t)\phi_0^\sigma(\alpha,x) = c_0^\sigma(0)\phi_0^\sigma(\alpha,x) . \qquad (A12)$$

On canceling $\phi_0(\alpha,x)$ from both sides (for infinitesimal α) we have

$$c_0^\sigma(t) = c_0^\sigma(0) . \qquad (A13)$$

Combine this with (A8) to get

$$I = c_0^\sigma(0) . \qquad (A14)$$

In other words, the overlap integral at all times remains equal to the amplitude of the $n = 0$ state at the initial time. For an initial occupation of any of the eigenstates of the regularized Hamiltonian (A3) in (13), $c_0^\sigma(0) = 0$, and from (A14), the overlap (A7) $I = 0$. Note that the relation (A13) has a simple physical meaning: an infinitely deep nondegenerate state, if occupied initially, will remain equally occupied at all times, since no finite amount of coupling can cause a transition.

[1] Q. Su and J. H. Eberly, J. Opt. Soc. Am. B **7**, 564 (1990).

[2] Q. Su, J. Eberly, and J. Javanainen, Phys. Rev. Lett. **64**, 862 (1990).

[3] V. C. Reed, P. L. Knight, and K. Burnett, Phys. Rev. Lett. **67**, 1415 (1991).

[4] J. Javanainen, J. H. Eberly, and Q. Su, Phys. Rev. A **38**, 3430 (1988).

[5] J. Grochmalicki, M. Lewenstein, and K. Rzążewski, Phys. Rev. Lett. **66**, 1038 (1991).

[6] M. Gajda, J. Grochmalicki, M. Lewenstein, and K. Rzążewski, Phys. Rev. A **46**, 1638 (1992).

[7] T. Ménis, R. Taieb, V. Véniard, and A. Maquet, J. Phys. B **25**, L263 (1992).

[8] R. Loudon, Am. J. Phys. **27**, 649 (1959). For a relativistic treatment, which seems to soften the effect of the singularity, see H. N. Spector and J. Lee, Am. J. Phys. **53**, 248 (1985), and the references cited therein.

[9] R. V. Jensen, Phys. Rev. Lett. **49**, 1365 (1982).

[10] Ue-Li Pen and T. F. Jiang, Phys. Rev. A **46**, 4297 (1992).

[11] W. H. Press, B. P. Flannery, S. A. Teukolsky, and W. T. Vetteling, *Numerical Recipes* (Cambridge University Press, Cambridge, England, 1987), p. 615.

[12] M. Pont, N. R. Walet, M. Gavrila, and C. W. McCurdy, Phys. Rev. Lett. **61**, 939 (1988).

[13] K. C. Kulander, K. J. Schafer, and J. L. Krause, Phys. Rev. Lett. **66**, 2601 (1991).

[14] H. A. Kramers, *Collected Scientific Papers* (North-Holland, Amsterdam, 1956); W. C. Henneberger, Phys. Rev. Lett. **21**, 838 (1968); F. H. M. Faisal, J. Phys. B **6**, L89 (1973).

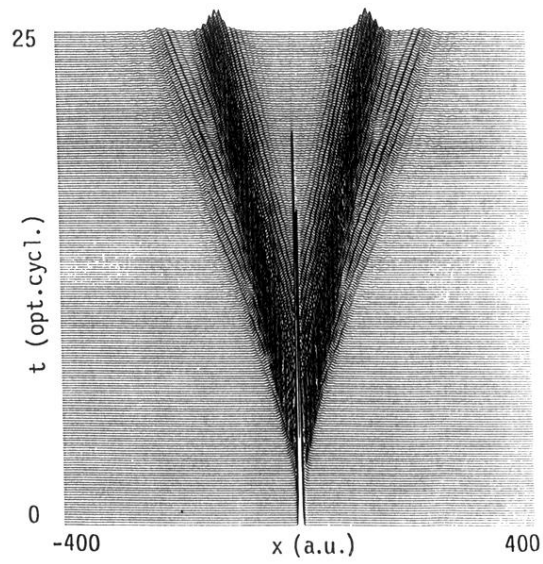[15] P. Agostini, F. Fabre, G. Mainfray, G. Petite, and N. K. Rahman, Phys. Rev. Lett. **42**, 1127 (1979).

FIG. 1. Probability density $|\psi(x,t)|^2$ of the "hard" Coulomb atom in the laser field; $\omega = 1$ (a.u.) and $E_0 = 0.5$ (a.u.) (perpendicular perspective).
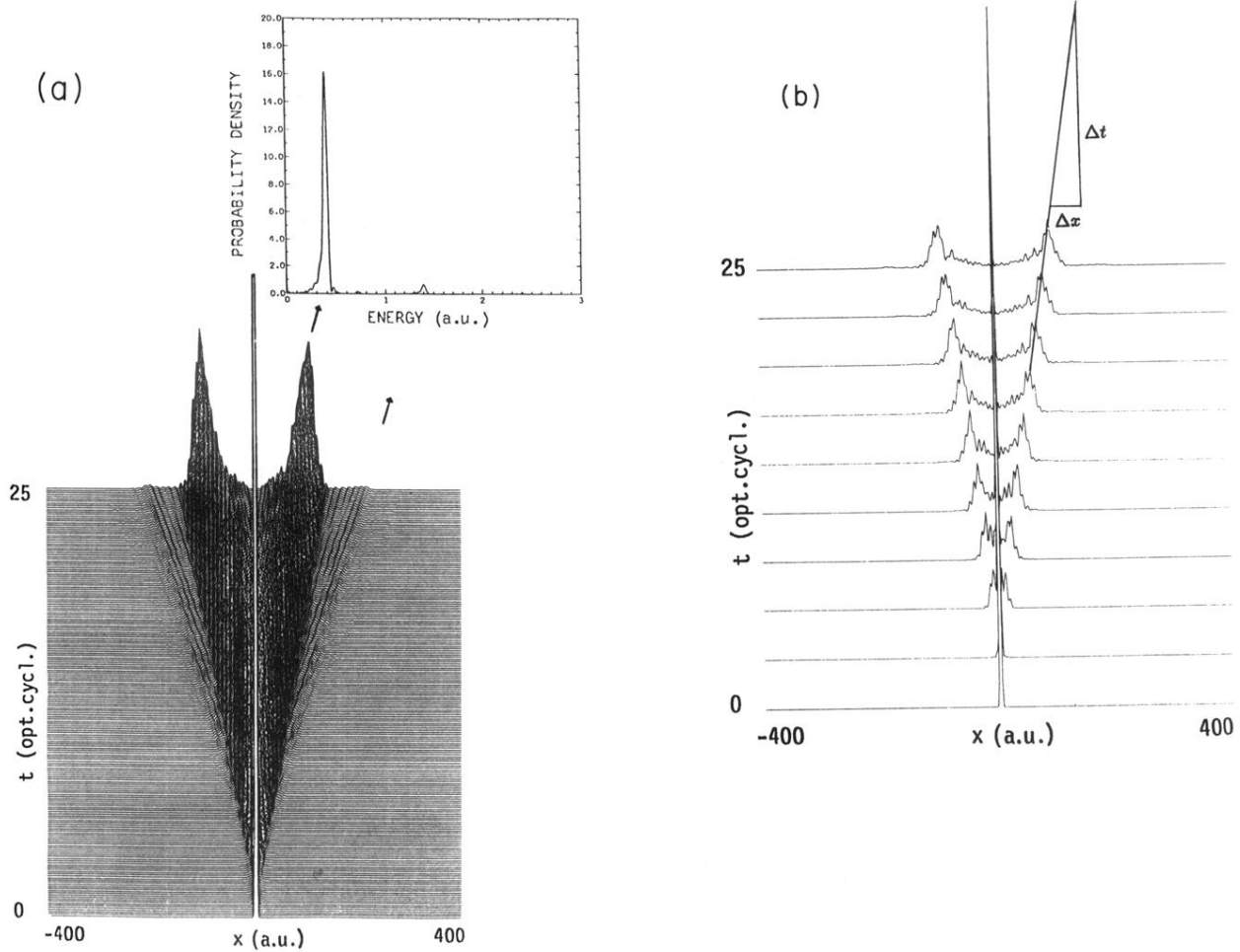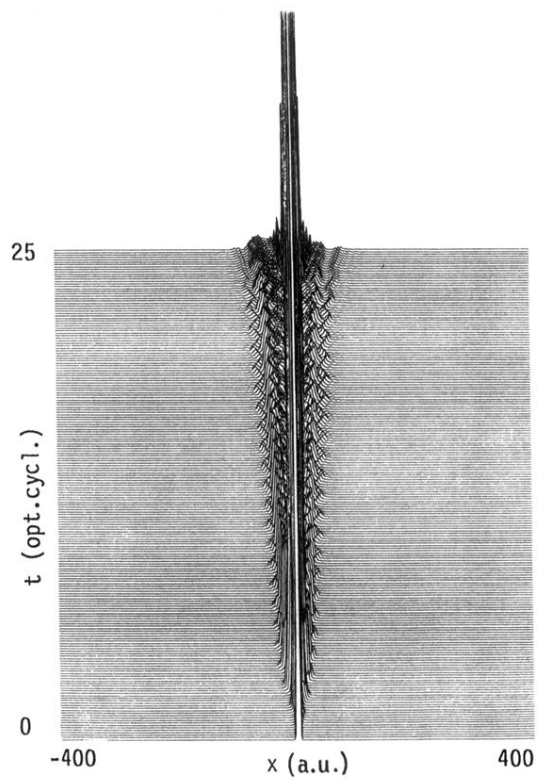
(a)

(b)

FIG. 10. (a) Probability density $\psi(x,t)|^2$ and the corresponding ATI spectrum of the "soft" Coulomb model; $\omega = 1$ (a.u.) and $E_0 = 1$ (a.u.). (b) Probability density as in (a), but with a reduced vertical scale and fewer time steps, which reveals the linear motion of the high-density group of the wavepackets more clearly.

FIG. 11. Probability density $|\psi(x,t)|^2$ of the "soft" Coulomb atom in the laser field; $\omega = 1$ (a.u.) and $E_0 = 10$ (a.u.).
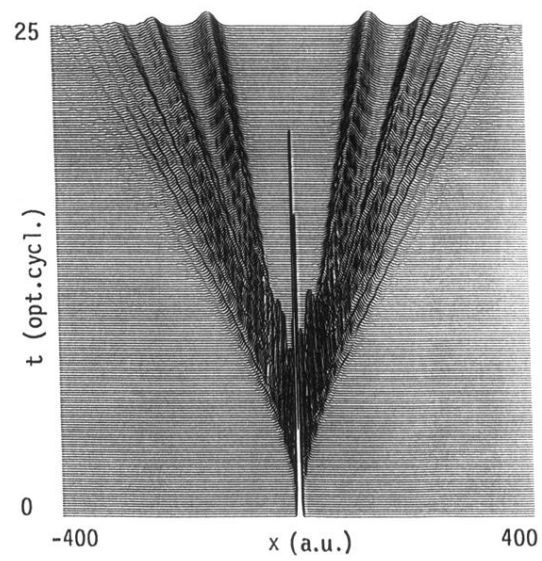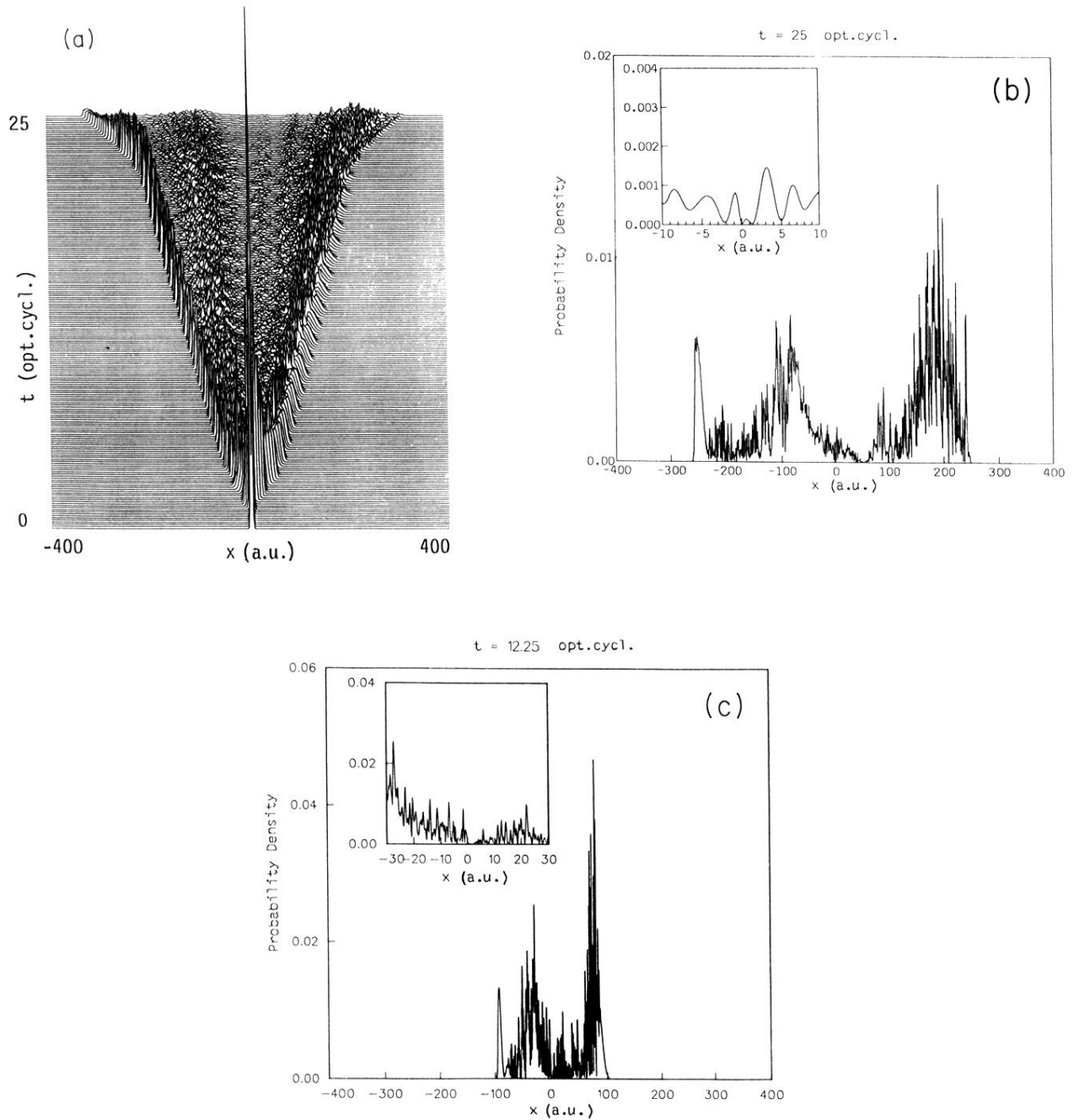
FIG. 2. Same as Fig. 1, but $E_0 = 1$ (a.u.).

FIG. 3. (a) Same as Fig. 1, but $E_0 = 10$ (a.u.). (b) Probability density at time $t = 25$ (optical cycles); $\omega = 1$ (a.u.), $E_0 = 10$ (a.u.). (c) Same as in (b), but $t = 12.25$ (optical cycles).
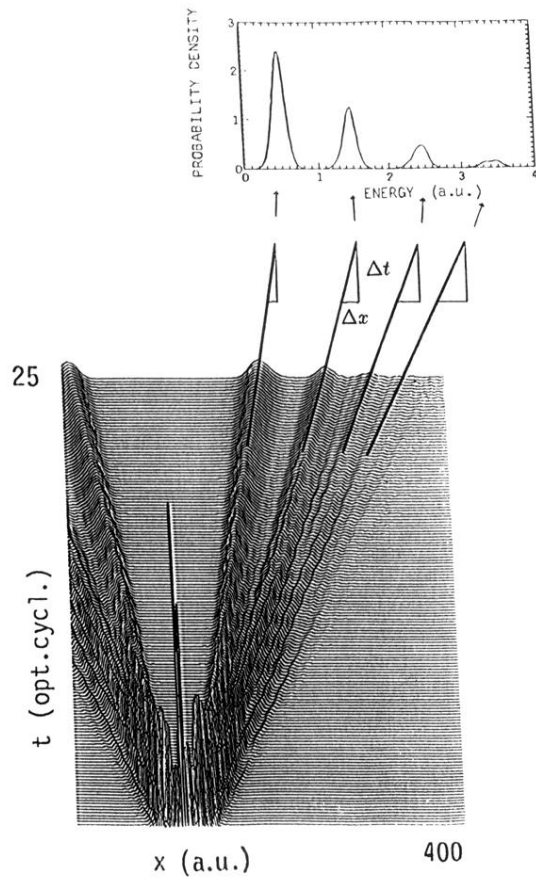
FIG. 7. Correlation between spatial subpackets, formed by wave-packet splitting, and the ATI peaks [$\omega = 1$ (a.u.) and $E_0 = 1$ (a.u.)]. The crest of each subpacket of the electron probability density moves with a velocity $v = \Delta x / \Delta t$; the associated kinetic energy $v^2/2$ can be identified with the energy of an individual peak in the ATI spectrum (indicated by an arrow).